Hindawi
Shock and Vibration
Volume 2019, Article ID 8202780, 11 pages
https://doi.org/10.1155/2019/8202780

Research Article

Experimental Investigation of Steel Plate Shear Walls under Shear-Compression Interaction

Yang Lv[1,2] **Ling Li**[1] **Di Wu**[1] **Bo Zhong**[3] **Yu Chen**[4] **and Nawawi Chouw**[1,2]

[1]*Tianjin Key Laboratory of Civil Structure Protection and Reinforcement, Tianjin Chengjian University, Tianjin 300384, China*
[2]*Department of Civil and Environmental Engineering, The University of Auckland, Auckland 1142, New Zealand*
[3]*Sichuan Fire Research Institute of MEM, Chengdu 610036, China*
[4]*Airport College, Civil Aviation University of China, Tianjin 300300, China*

Correspondence should be addressed to Yu Chen; tjucy@tju.edu.cn

Received 23 September 2018; Revised 9 January 2019; Accepted 21 February 2019; Published 18 March 2019

Academic Editor: Sundararajan Natarajan

Four scaled one-storey single-bay steel plate shear wall (SPSW) specimens with unstiffened panels were tested to determine their behaviour under cyclic loadings. The shear walls had moment-resisting beam-to-column connections. Four different vertical loads, i.e., 300 kN, 600 kN, 900 kN, and 1200 kN, representing the gravity load of the upper storeys were applied at the top of the boundary columns through a force distribution beam. A horizontal cyclic load was then applied at the top of the specimens. The specimen behaviour, envelope curves, axial stress distribution of the infill steel plate, and shear capacity were analyzed. The axial stress distribution and envelope curves were compared with the values predicted using an analytical model available in the literature.

1. Introduction

To investigate the shear resistance of single-bay steel plate shear walls (SPSWs), a large number of experiments have been conducted using low cyclic loading. Driver et al. [1] carried out a cyclic test of a four-storey SPSW. A vertical load of 720 kN was applied at the top the of the boundary columns with one horizontal load at each floor level. Their results indicated that the final deflection at the top floor is nine times larger than the yield deflection. The test specimen proved to be initially very stiff and had an excellent ductility and energy dissipation. Later, because of damage to the 1st storey, only the upper three storeys of this SPSW specimen was further tested by Behbahanifard [2] to verify their finite element model. Moghimi and Driver [3] carried out a test of a large-scale two-storey SPSW specimen. A vertical load was also considered in their test. The results indicated an excellent performance. In addition, high ductility and energy dissipation were observed. Qu et al. [4] performed a two-phase experimental program on a full-scale two-storey SPSW with reduced beam section connections and composite floors. Their first-phase test was pseudodynamical tests using three ground motions of decreasing intensity. The buckled infill steel plate was replaced by new panels in the subsequent test. Their results showed that the repaired specimen could survive and dissipate significant energy without severe damage to the boundary frame. The final storey drifts reached 5.2% and 5.0% at the first and second storey. Other experimental research included works on reduced beam section anchor [5], low-yield point SPSW [6], unstiffened perforated SPSWs [7], partially connected SPSWs [8], SPSWs with semirigid connected frame [9], shake table test of buckling restrained SPSWs [10], self-centering SPSW [11], and the use of light-gauge SPSWs [12].

However, until today, physical experiments on the cyclic behaviour of SPSWs under concurrent gravity and horizontal load have not been reported. Most investigations were performed numerically, e.g., Elgaaly and Liu [13] compared the shear carrying-capacity of a SPSW with and without gravity load by the finite element method. The authors concluded that the gravity load has little effect on the shear-carrying capacity. This might be caused by the low magnitude of compression and thin infill wall considered in their analyses. Zhang and Guo [14] performed finite element

analyses on the behaviour of SPSWs with precompression from the adjacent columns. Their research showed that the shear capacity of SPSWs was significantly impaired by the precompression. Their previous research [15] also showed that the gravity load acting at the top of the boundary columns has significant effects on the shear load-carrying capacity.

To evaluate the adequacy of an analytical model available in the literature in predicting the influences of gravity loads on the cyclic performance of the SPSW, physical experiments were performed in this paper. Four scaled SPSWs under compression-shear interaction were designed and tested. The envelope curves, the axial stress distribution and the maximum shear capacity obtained from the experiments were then used in the evaluation of the analytical model.

2. Specimens and Test Setup

The test parameter was the vertical load applied at the top boundary columns. Test specimens are one-storey walls. The height of the specimen was 0.75 m, and the width was 1.1 m. The columns were 1 m apart from center to center. Figure 1 shows the size and configuration of the specimens. The plate thickness was 2.1 mm Q235 steel with the yield strength of 255 MPa. The size of the infill plate was 600 mm × 900 mm. The frame members are built-up sections made of Q345 steel with the yield strength of 460 MPa. The boundary columns, i.e., H-overall depth (d) × flange width (b_f) × web thickness (t_w) × flange thickness (t_f), have, respectively, the dimensions of 100 mm × 100 mm × 6 mm × 8 mm. The top beam, connected to the actuator, has the corresponding dimensions of 150 mm × 100 mm × 6 mm × 9 mm. This beam was stiff to ensure a smooth transfer of the load to the tension field occurred below the beam. Moment connections were used at all beam-to-column joints. Connection of the beam flanges to the columns was constructed using complete penetration groove welds. The beam webs were welded to the column flange by two-sided fillet. The infill steel plate was connected to the boundary beams and columns using the fishplates. Figure 2 shows the fishplates of 50 mm width and 3 mm thickness. Continuous fillet welds on both sides of the fishplates were used. The infill steel plate is fitted to the fishplates with a lap of approximately 20 mm all around.

Figure 1 shows a sketch of the test specimen with the vertical load and the lateral cyclic load. The constant vertical load of specimens A, B, C, and D was, respectively, 300 kN, 600 kN, 900 kN, and 1200 kN. It was kept steady during the whole test. The beam that distributed the vertical load was hinged to the top of the two boundary columns. A hydraulic jack generated the vertical load at the top of the load distribution beam. It was supported by a stiff steel frame. To avoid any shear force, a roller was placed between the steel frame and the hydraulic jack.

Horizontal cyclic load acted at the center line of the top beam. A hydraulic jack, supported by a laboratory reaction wall, generated the horizontal load. Up to the first yield in the steel plate, a force-controlled load was applied. Depending on the load combination, the first yielding stage was achieved by increasing the horizontal load from ±50 kN to ±200 kN with an increment of 50 kN. In the subsequent load cycles, a displacement-controlled loading was performed until the specimen failure by increasing the displacement after each three cycles from ±4 mm.

Eighteen strain gauges were attached along the boundary columns to measure the axial strain, and 8 strain rosettes were attached at the surface of the infill steel plate (see Figure 1). Two linear variable differential transformers (LVDTs) were installed at the base of the boundary column and at the center line of the top beam.

Table 1 lists the results of the coupon tests of the two materials Q345 and Q235. Three coupons were tested for each material, and the average value is used for the subsequent analytical analyses.

3. Test Results

3.1. Specimens Behaviour. Under pure gravity loads, no buckling occurred in specimens A, B, and C. However, in the case of specimen D, horizontal buckling of the infill steel plate took place. The following described the behaviour of the four specimens.

In the case of specimen A, until the top displacement reached 4 mm, there was no buckling in the infill steel plate. The tension strips, formed from the lower left corner to the upper right corner, have an inclination angle near to 45°. During the first displacement cycle of 8 mm, the first loud bangs occurred. In the subsequent cycles, these noises continued to occur. With an increase of the top displacement, various parts of the infill steel plate progressed to yield. A large residual deformation formed at the end of each pull or push loading with a further increase of residual deformation in the subsequent cycles. The first tear was detected in the upper left corner between the fishplate and the infill steel plate during the first 12 mm displacement load. The tear gradually increased to nearly 30 mm at the end of the first 12 mm cycles, as shown in Figure 3. At the end of the second 12 mm displacement cycle, new tears were detected at the two lower corners. All the tears extended with an increase of the top displacement, but no new tear was observed. During the first 20 mm displacement cycle, the shear resistance of the specimen did not decrease, but the tears grew faster and the specimen was pushed over. The ultimate deformation at the top of the specimen reached more than 50 mm. The force resistance only dropped by about 15%. At the end of the test, all the tears extended to be more than 60 mm. The tension boundary column failed due to the rupture of the weld at the bottom of the column, as shown in Figure 4. Meanwhile, the compression column experienced local buckling in the flange, and only a slight out-of-plane deformation was observed.

In the case of specimen B, i.e., under 600 kN vertical load, no buckling or yielding was detected. Prior to reaching the yield displacement, four load cycles with increasing magnitude from ±50 kN to ±200 kN were necessary to cause the first yielding. At the cyclic load of 150 kN, the first loud bang occurred. These noises also occurred during the unloading phase in the following cycles. However, tension strips first

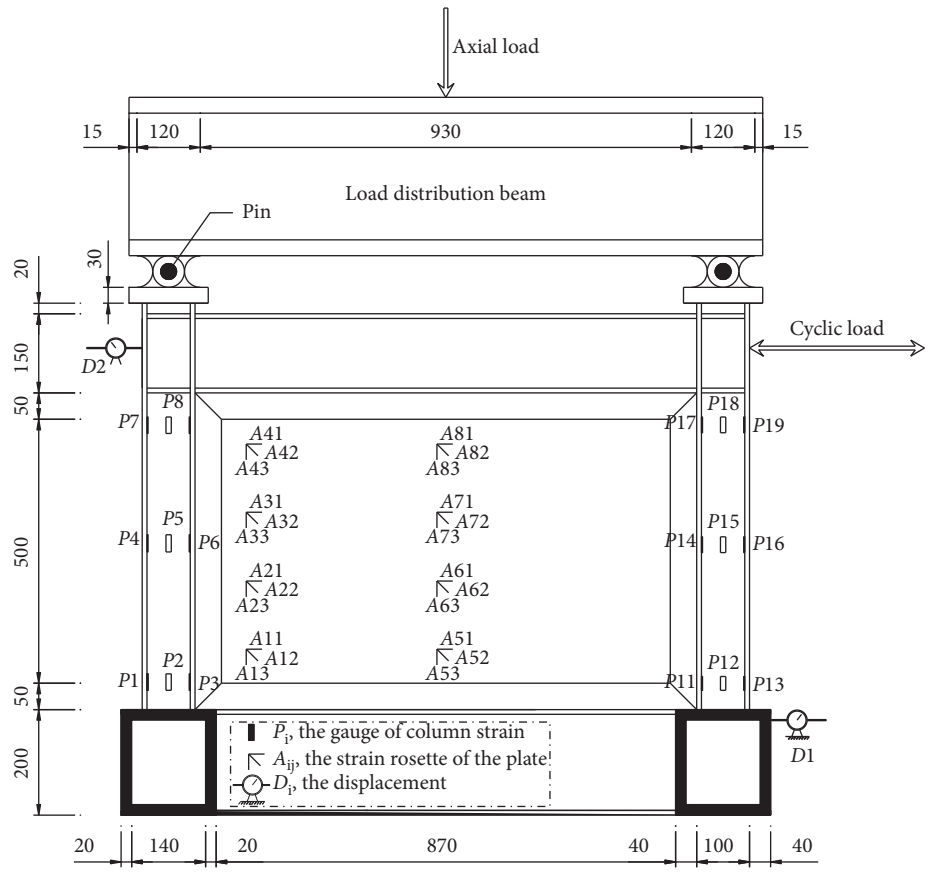

Figure 1: Dimensions of specimens (units: mm) and layout of strain gauges and LVDTs.

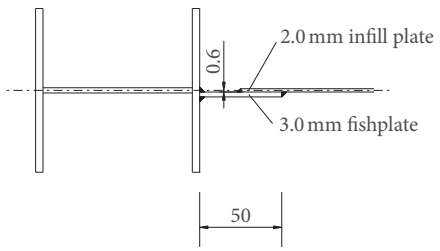

Figure 2: Details of the fishplate (units: mm).

only occurred during the second cycle of the 2 mm level, as indicated by the diagonal lines in Figure 5. The first tear was detected at the upper left corner at the end of the third cycle of 4 mm. The length of the tear was about 10 mm, and this tear gradually grew in the following cycles. At the first 6 mm displacement cycle, new tears of about 15 mm length occurred at the upper right and lower left corners. The length of the tear at the upper left corner extended to about 20 mm. At the end of the second 10 mm displacement cycle, a slight buckling at the support of the boundary column under compression was observed. The length of tear at the upper right corner extended to about 50 mm. At the second 12 mm displacement cycle, as shown in Figure 6, the upper left tear extended to nearly 60 mm, and the shear force resistance did not decrease. During the first 16 mm displacement pull load, the specimen reached a maximum resistance at the top displacement of 13 mm. The shear resistance then began to decrease. At the second 16 mm displacement cycle, the shear resistance decreased rapidly. The failure started at the support of the column under compression where a significant buckling and yield occurred. An out-of-plane deformation increased very fast, resulting in a loss of the in-plane shear resistance.

In the case of specimen C, soft noises occurred during the application of the vertical load of 900 kN, even prior to the horizontal load. However, no buckling and yielding were detected. Prior to reaching the yield displacement, three load cycles with increasing magnitude from ±50 kN to ±150 kN were necessary to cause the first yielding. The first loud bang occurred at the cycle of 150 kN. The tension strips occurred while pushing. After unloading, a large residual deformation was observed. At the first 6 mm displacement cycle, a first vertical tear occurred at the upper left corner. In the following load cycle, a new tear occurred at the upper right corner at the compression direction. At the first 8 mm displacement cycle, local buckling of the compression column appeared. The shear resistance did not decrease. At the second 8 mm displacement cycle, the tear at the upper left corner extended to about 40 mm. The global out-of-plane buckling occurred, and the shear resistance of the specimen decreased rapidly to less than 100 kN. Specimen C failed because of the global out-of-plane buckling, as shown in Figure 7.

Table 1: Results of tensile coupon test.

Steel	Nominal thickness (mm)	Actual thickness (mm)	Yield stress (MPa)	Ultimate stress (MPa)	Gauge length (mm)	Elongation at rupture (%)	Yield strength ratio
Q345	6/8	6/8	460	567	225	21.2	0.81
Q235	2	2.1	255	375	225	18.5	0.68

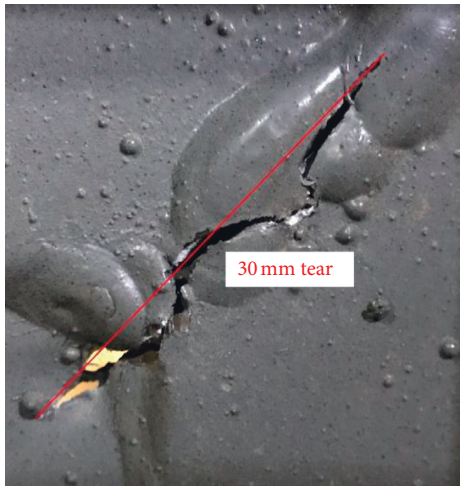

Figure 3: Tear at the interface between fish and infill steel plates at the end of 12 mm cyclic load.

In the case of specimen D, a soft noise occurred when the vertical load reached 900 kN, and no buckling and yielding were observed in the specimen. The vertical load gradually increased to 1200 kN. The noises increased, but there was no loud bang. Slight horizontal waves due to buckling of the infill steel plate occurred. The first bang occurred at the 50 kN horizontal load cycle. These noises occurred several times during each cycle in the following load cycles. After the 150 kN load cycle, a displacement loading was applied. The shear resistance capacity was stable at 2 mm and 4 mm displacement cycles, and there were no tear. At the 6 mm displacement cycles, the shear resistance began to decrease during the pulling. The reason was the anchorage of the column under compression failed (Figure 8(a)). The failure mode is shown in Figure 8(b).

3.2. Envelope Curves. Figure 9 shows the envelopes of the load-top displacement. It should be noted that specimen A was pushed over after three 20 mm displacement cycles. In the early load cycles, the infill steel plate behaved in an elastic manner (see Figure 9). As the deformation increased, part of the infill steel plate yielded, resulting in a gradually decreasing stiffness. After significant yielding of the infill steel plate, unloading and reloading produced a consistent hysteresis loop. During the cyclic load, severe pinching did not occur, and the steel plates dissipated a considerable energy [16]. The deformation capacity was also excellent. The maximum storey drift δ_{max}/H for specimen A was 7%. However, the deformation capacity was significantly decreased with an increase of the vertical load. The maximum storey drifts for specimens B, C, and D were, respectively, 2.42%, 1.39%, and 1.22%. It should be noted that the failure mode of specimens C and D was due to the global out-of-plane buckling.

To make it easier to understand, the characteristic results, the initial yield point (δ_{yi}, F_{yi}), the maximum shear resistance F_{max}, and corresponding displacement δ_p, referenced in [16], are shown in Table 2.

From Table 2, it is clear that the maximum shear resistance decreases with an increase of the vertical load. Specimen A experienced excellent deformation capacity, even in the case of the top displacement reaching 51 mm. The shear resistance only decreased by about 15%. Prior to the 16 mm displacement cycles, specimen B behaved similar to A. During the 16 mm displacement cycle, the specimen experienced unstable and decreased shear resistance. The failure mode of specimen B was the buckling of the column base and long tears at the corners of the infill steel plate. In the case of specimens C and D, the initial stiffness under the positive loading was, respectively, 88.1 kN/mm and 57.8 kN/mm and under the negative loading 79.5 kN/mm and 62.1 kN/mm. The shear resistance of C and D was much smaller than that of specimens A and B. One reason was that the vertical load, acting at the top of the boundary columns, decreased the yield stress of the infill steel plate more than that in the case of specimens A and B. The other reason was both specimens C and D failed because of the out-of-plane buckling of the compressed column.

3.3. Available Analytical Approach [17, 18]. The analytical model in reference [17], as shown in Figure 10, under gravity load the stress distribution of the infill plate is assumed to be symmetric. The maximum stress in the vertical direction adjacent to the boundary columns is assumed to be the axial stress of the boundary columns. The infill plate is idealized to be clamped along all edges and subjected to a uniform compressive stress due to the top boundary beam. The maximum vertical stress of the inner part of the plate is assumed to be an elastic buckling stress. The buckling stress can be calculated by

$$\sigma_{cr} = k\frac{\pi^2 E}{12\left(1-\mu^2\right)(L/t)^2}, \tag{1}$$

where k is the buckling coefficient and has the value of

$$k = 3.6 + 4.3\left(\frac{L}{H}\right)^2 + 2.5\left(\frac{H}{L}\right)^2, \tag{2}$$

where H and t are the height and thickness of the infill steel plate and μ and E are Poisson's ratio and modulus of elasticity of the steel, respectively.

As shown in Figure 10, zone I [17] is the precompression influenced area, and the width equals to L_e, which is the

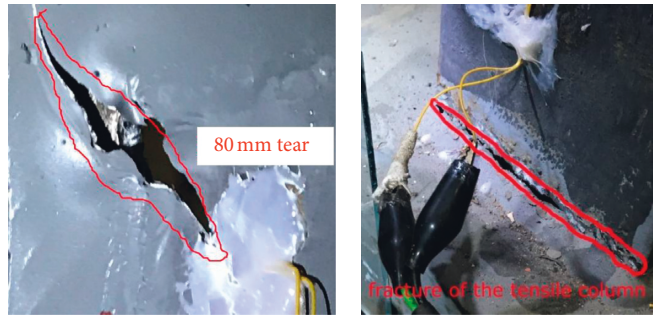

(a) (b)

Figure 4: At the end of the test: (a) tear at the upper left corner and (b) failure at the support of the column in tension.

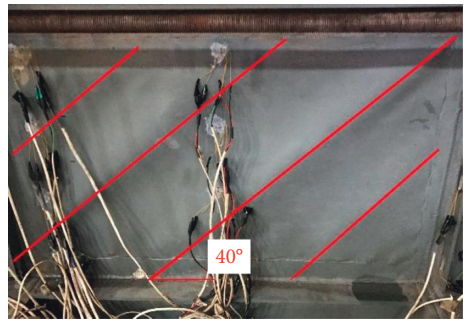

Figure 5: Formation of tension strips in infill steel plate.

(a) (b)

Figure 6: Failure mode of specimen B. (a) Tear at the upper left during the second 12 mm load cycle of and (b) local buckling of the column in compression.

effectiveness width of the web plate [17]. Zone II is the precompression uninfluenced area. The inclination angle α_I of tension strip in zone I is calculated based on the energy conservation:

$$\alpha_I = \tan^{-1}\sqrt[4]{\left[(\gamma+1)^2+\frac{tL_e}{2A_c}\right]\left[1+tH\left(\frac{1}{A_b}+\frac{H^3}{360I_cL^2}\right)\right]^{-1}}, \quad (3)$$

where H is the height of the plate and A_c and A_b are, respectively, the section areas of the column and beam. I_c is the moment inertia of the column, and γ is a parameter defined as the ratio of gravity load and the shear-induced axial force in the infill steel plate:

$$\gamma = \frac{P_g}{f_{y,p}tL\cos^2\alpha_0}, \quad (4)$$

where α_0 is the inclination angle of the tension strip without vertical load, P_g is the gravity load of the columns, $f_{y,p}$ is the yield stress of the plate, and t and L are, respectively, the thickness and width of the plate.

The inclination angle α_{II} [17] of tension strip in zone II is

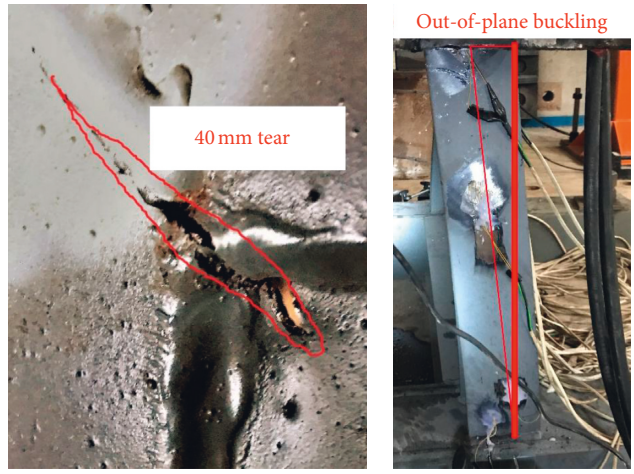

(a) (b)

Figure 7: Damage to the end of the test of specimen C. (a) Tear at the upper left corner and (b) the failure mode.

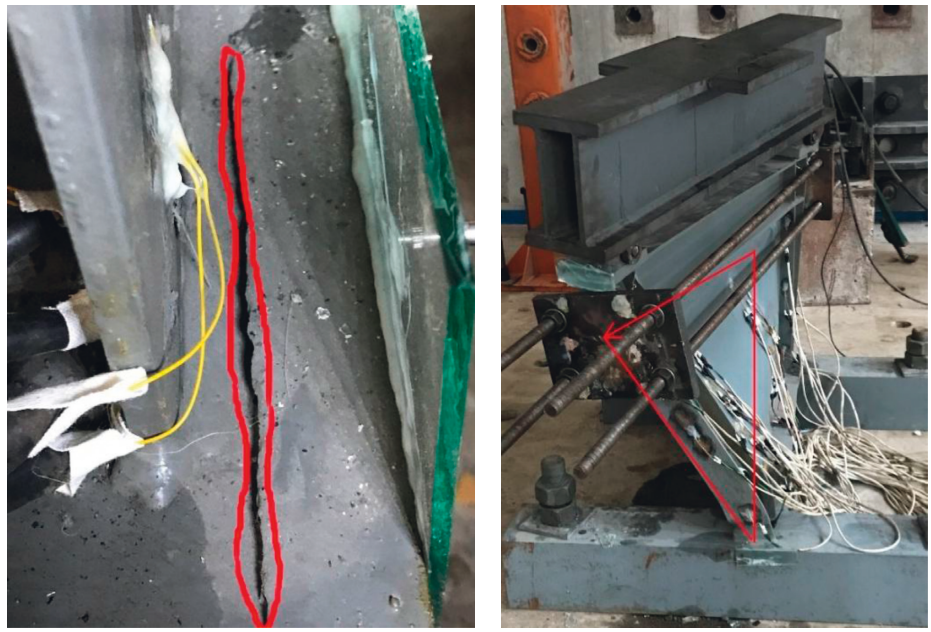

(a) (b)

Figure 8: Failure mode of specimen D. (a) Fracture at the support of the column under compression and (b) global out-of-plane buckling of the specimen.

$$\alpha_{II} = \tan^{-1}\sqrt[4]{\left[1+\frac{t\left(L-L_e\right)}{2A_c}\right]\left(1+\frac{tH}{A_b}\right)^{-1}}. \quad (5)$$

Figure 11 shows the stress and tension strips of the infill steel plate under shear and compression. The yield stress [18] of the tension strips of zone I $\sigma_{ty,I}$ and zone II $\sigma_{ty,II}$ can be calculated as

$$\sigma_{ty,I} = \frac{\sigma_{v,p}^{max}\left(3\sin^2\alpha_I - 1\right) + \sqrt{\left[\sigma_{v,p}^{max}\left(3\sin^2\alpha_I - 1\right)\right]^2 - 4\left[\left(\sigma_{v,p}^{max}\right)^2 - f_{y,p}^2\right]}}{2},$$
$$\sigma_{ty,II} = \frac{\sigma_{crv,p}\left(3\sin^2\alpha_{II} - 1\right) + \sqrt{\left[\sigma_{crv,p}\left(3\sin^2\alpha_{II} - 1\right)\right]^2 - 4\left[\left(\sigma_{crv,p}\right)^2 - f_{y,p}^2\right]}}{2}, \quad (6)$$

Table 2: Characteristic results [16].

Specimen	Positive loading						Negative loading					
	F_{max}	δ_{max}	F_y	δ_y	F_{yi}	δ_{yi}	F_{max}	δ_{max}	F_y	δ_y	F_{yi}	δ_{yi}
A	334.0	18.32	257.2	5.91	80.0	0.93	334.5	20.15	246.0	6.1	80.0	0.86
B	320.5	16.65	247.2	6.53	102.2	0.95	318.8	18.03	265.3	6.21	100.9	0.99
C	230.9	8.10	197.3	4.7	55.5	0.63	239.0	6.94	190.6	4.63	50.9	0.64
D	146.9	3.49	146.9	3.49	51.4	0.89	190.5	5.73	151.3	3.83	50.3	0.81

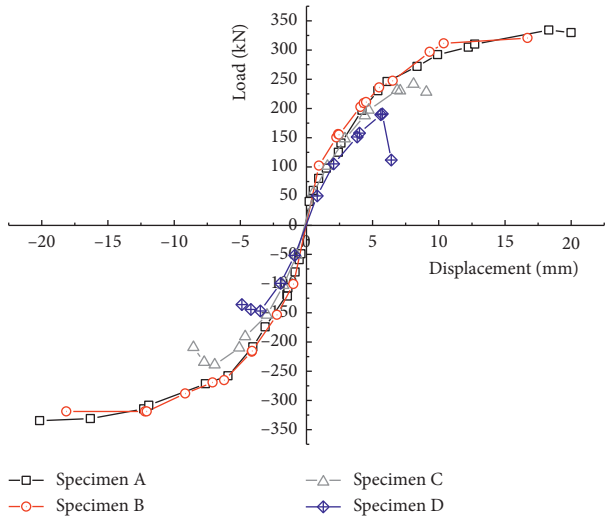

Figure 9: Envelopes of load-top displacement curve of test specimens (reproduced with permission from Lv et al. [16]).

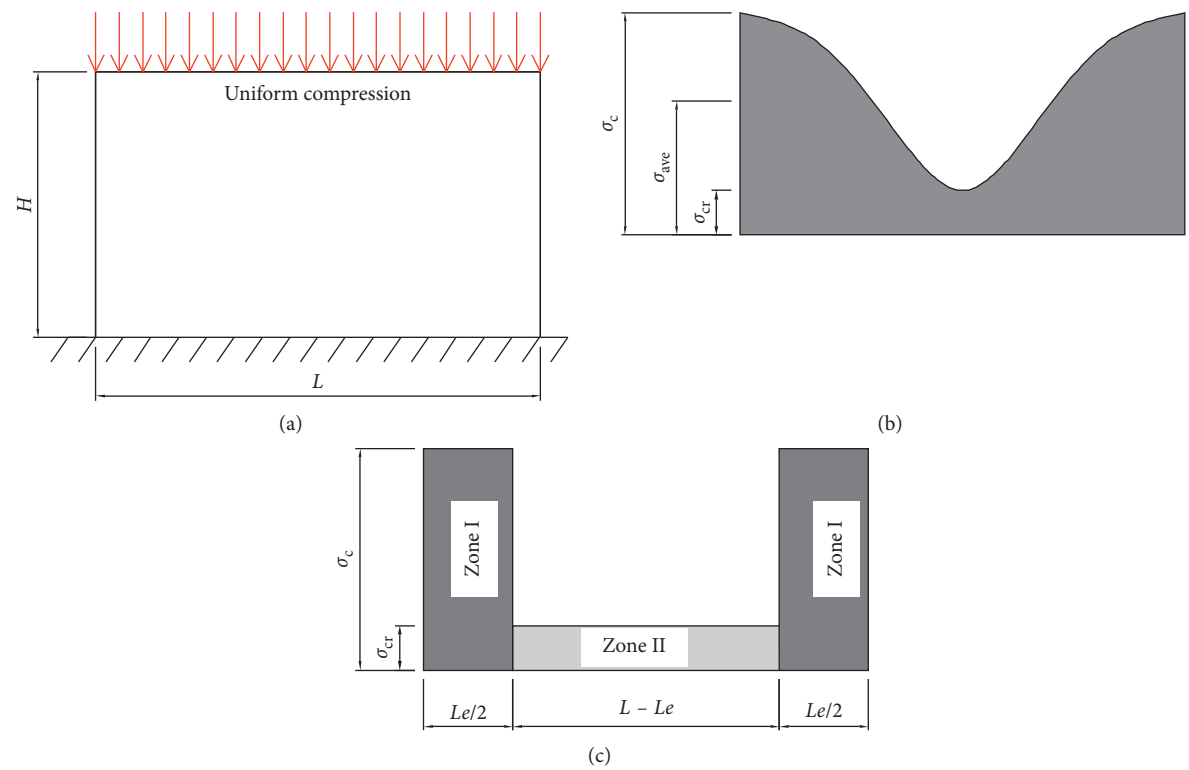

Figure 10: Schematic diagram of the equivalent compression stress after elastic buckling.

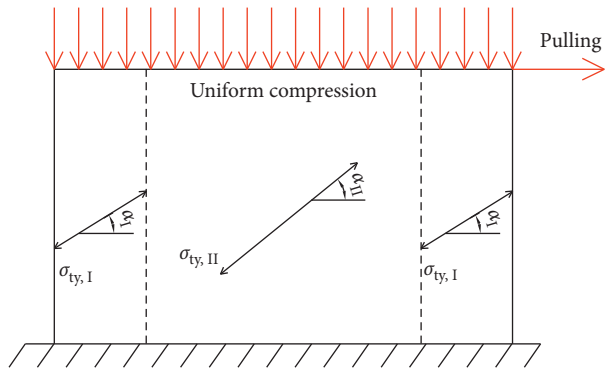

Figure 11: Yield stress of the infill steel plate under compression and shear.

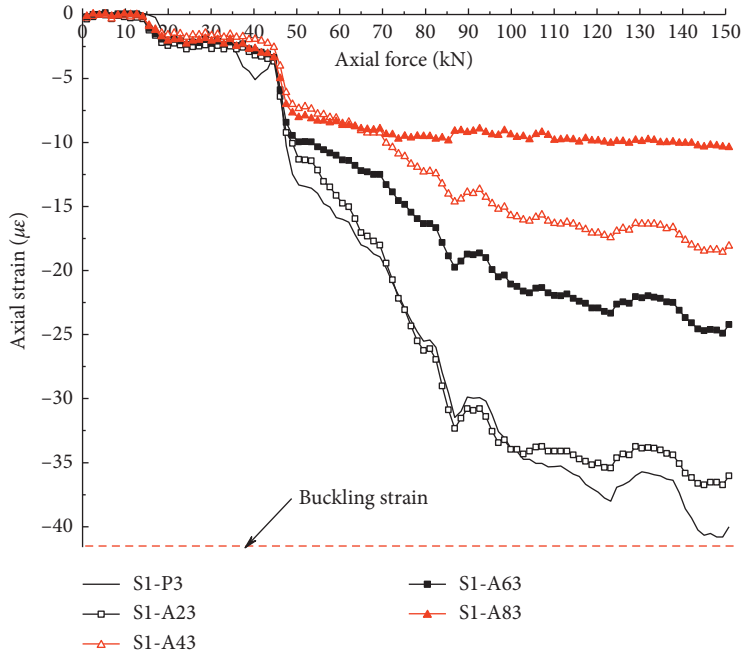

(a)

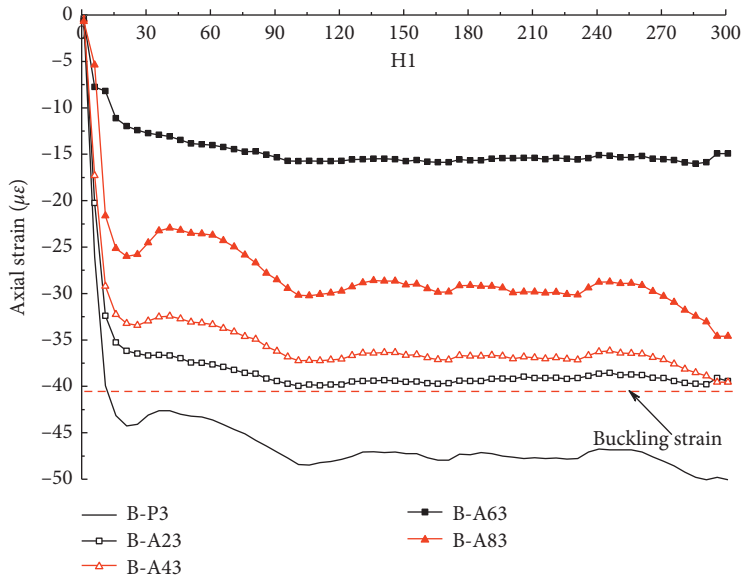

(b)

Figure 12: Continued.

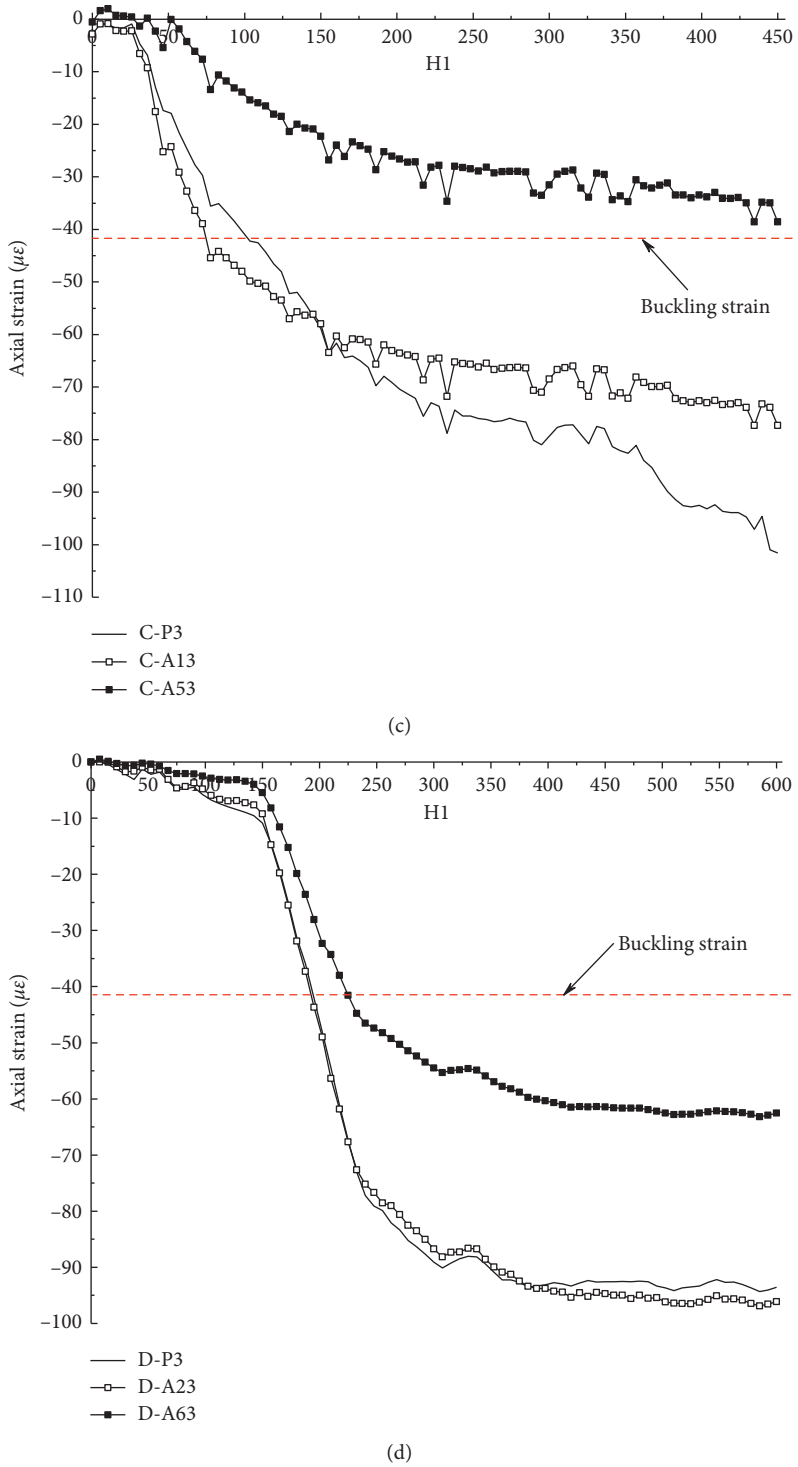

Figure 12: Comparison of the distribution of axial strains and the buckling strain under pure gravity load.

where $\sigma_{v,p}^{max}$ is the maximum vertical stress of the plate which is idealized to be equal to the axial stress of the column.

Based on the above assumption, the shear resistance of zone I $V_{sp,I}$, zone II $V_{sp,II}$, and the boundary frame V_{sf} can be calculated. The shear force capacity V_s of the SPSW is the sum of that of the infill steel plate V_{sp} and that of the boundary frame V_{ff}, which has the values of

$$V_{sp} = V_{sp,I} + V_{sp,II} = \sigma_{ty,I} L_e t \sin\alpha_I \cos\alpha_I + \sigma_{ty,II}(L - L_e) t \sin\alpha_{II} \cos\alpha_{II},$$
$$V_{ff} = \frac{A_c(f_{y,c} - \sigma_{g,c})l}{h} - \frac{P_g \delta_p}{H}, \quad (7)$$

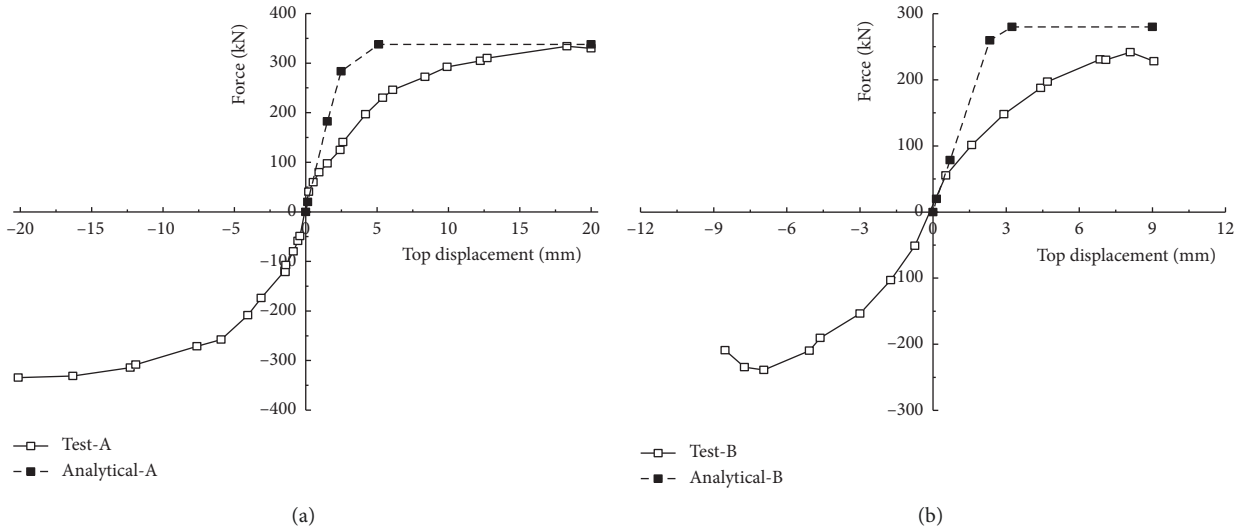

Figure 13: Envelope curves of test and predicted curves for (a) specimen A and (b) specimen B.

where δ_p is the displacement of the SPSW corresponding to the maximum shear resistance. Details of the considered analytical model are given in references [17, 18].

4. Comparison between Experimental and Analytical Results

Figure 12 shows the axial strain of the boundary column and the infill steel plate under vertical load, i.e., prior to the horizontal load. P3 is the strain measured at the middle height of the boundary column. A13, A23, and A33 are measured at the infill steel plate next to the boundary columns. A53, A63, and A83 are measured at the middle of the infill steel plate (see Figure 1). The strain of the boundary column P3 and that of the infill steel plate near to the boundary column A23 are almost the same. The results show that the stress of the boundary column and the infill steel plate next to the columns can be assumed to be identical. The strains at the middle of the infill steel plate are smaller than these at the boundaries. Based on equation (1), the buckling stress of the infill steel plate is 8.57 MPa, and the corresponding buckling strain is about 41.6 $\mu\varepsilon$. The results show that the analytical buckling strain of specimen C provides the best prediction. For specimen A, the predicted strain is much larger because the infill steel plate does not buckle when the vertical load is 150 kN. In the case of specimen D, the strain gauges may be located at the valley or peak of the buckling; thus, the measured strain is much larger than the predicted value.

Figure 13 shows the envelope curves of the load-top displacement relationships of the specimens A and B. It is clear that the stiffness from the predicted model is higher than that of the test. Under a small axial stress, specimens A and B experienced ductile behaviour. This is indicated by a good load resistance during the lateral displacement.

Table 3 shows that the predicted shear strength of specimen A is close to the test result. Specimen B has a predicted value lower than that of the testing result, while the predicted strength of specimens C and D is larger than those of the testing results. The reasons are specimens C and D failed due to the global out-of-plane buckling of the columns. This failure mode cannot be considered in the analytical model.

Table 3: The predicted shear capacity of the specimens.

Specimen	δ (mm)	α (°)	L_e (mm)	$2V_{sp,I}$ (kN)	$V_{sp,II}$ (kN)	V_{sf} (kN)	V_s (kN)	Test (kN)
A	20.2	41.7	238	36	204	97.7	338	**334**
B	18.0	38.0	207	14	212	80.6	307	**320**
C	8.1	35.0	192	0	217	63.5	280	**249**
D	5.73	32.7	192	0	222	46.4	263	**191**

5. Conclusions

Four scaled SPSWs with different vertical loads at the top of the boundary columns were tested. The goal was to investigate the influence of gravity load on the cyclic performance of the SPSWs.

The findings obtained in the tests are summarized as follows:

(1) The shear resistance capacity of the SPSW decreases with an increase of the vertical load.

(2) The failure mode of specimens under heavy gravity load (cases C and D) is due to global out-of-plane buckling. This behaviour cannot be predicted by the analytical model.

(3) The analytical model overestimates the stiffness of SPSW.

(4) The model can predict the axial stress distribution of the infill steel plate.

Data Availability

The data used to support the findings of this study are available from the corresponding author upon request.

Conflicts of Interest

The authors declare that they have no conflicts of interest.

Acknowledgments

The authors gratefully acknowledge the partial support of this research by the National Key Research and Development Program of China under grant no. 2016YFC0701100, the National Natural Science Foundation of China under grant nos. 51808380, 51808129, and 51578361, and the Tianjin Basic Research Program under grant nos. 16JCZDJC38900 and 15JCZDJC39900. The authors also thank China Scholarship Council for supporting a one-year research stay of the first author at the University of Auckland.

References

[1] R. G. Driver, G. L. Kulak, D. J. L. Kennedy, and A. E. Elwi, "Cyclic test of four-story steel plate shear wall," *Journal of Structural Engineering*, vol. 124, no. 2, pp. 112–120, 1998.

[2] M. R. Behbahanifard, *Cyclic behavior of unstiffened steel plate shear walls*, Ph.D. dissertation, Department of Civil Engineering, University of Alberta, Edmonton, AB, Canada, 2003.

[3] H. Moghimi and R. G. Driver, "Economical steel plate shear walls for low-seismic regions," *Journal of Structural Engineering*, vol. 139, no. 3, pp. 379–388, 2013.

[4] B. Qu, M. Bruneau, C.-H. Lin, and K.-C. Tsai, "Testing of full-scale two-story steel plate shear wall with reduced beam section connections and composite floors," *Journal of Structural Engineering*, vol. 134, no. 3, pp. 364–373, 2008.

[5] D. Vian, M. Bruneau, K. C. Tsai, and Y.-C. Lin, "Special perforated steel plate shear walls with reduced beam section anchor beams. I: experimental investigation," *Journal of Structural Engineering*, vol. 135, no. 3, pp. 211–220, 2009.

[6] S.-J. Chen and C. Jhang, "Experimental study of low-yield-point steel plate shear wall under in-plane load," *Journal of Constructional Steel Research*, vol. 67, no. 6, pp. 977–985, 2011.

[7] T. M. Roberts and S. Sabouri-Ghomi, "Hysteretic characteristics of unstiffened perforated steel plate shear panels," *Thin-Walled Structures*, vol. 14, no. 2, pp. 139–151, 1992.

[8] M.-W. Wei, J. Y. Richard Liew, D. Yong, and X.-Y. Fu, "Experimental and numerical investigation of novel partially connected steel plate shear walls," *Journal of Constructional Steel Research*, vol. 132, no. 5, pp. 1–15, 2017.

[9] H. Guo, Y. Li, G. Liang, and Y. Liu, "Experimental study of cross stiffened steel plate shear wall with semi-rigid connected frame," *Journal of Constructional Steel Research*, vol. 135, pp. 69–82, 2017.

[10] M. Ge, J. Hao, J. Yu, P. Yan, and S. Xu, "Shaking table test of buckling-restrained steel plate shear walls," *Journal of Constructional Steel Research*, vol. 137, pp. 254–261, 2017.

[11] L. Xu, J. Liu, and Z. Li, "Behavior and design considerations of steel plate shear wall with self-centering energy dissipation braces," *Thin-Walled Structures*, vol. 132, pp. 629–641, 2018.

[12] J. W. Berman and M. Bruneau, "Experimental investigation of light-gauge steel plate shear walls," *Journal of Structural Engineering*, vol. 131, no. 2, pp. 259–267, 2005.

[13] M. Elgaaly and Y. Liu, "Analysis of thin-steel-plate shear walls," *Journal of Structural Engineering*, vol. 123, no. 11, pp. 1487–1496, 1997.

[14] X. Zhang and Y. Guo, "Behavior of steel plate shear walls with pre-compression from adjacent frame columns," *Thin-Walled Structures*, vol. 77, no. 4, pp. 17–25, 2014.

[15] Y. Lv and Z. X. Li, "Influences of the gravity loads on the cyclic performance of unstiffened steel plate shear wall," *The Structural Design of Tall and Special Buildings*, vol. 25, no. 17, pp. 988–1008, 2016.

[16] Y. Lv, L. Li, D. Wu, Y. Chen, Z.-x. Li, and N. Chouw, "Shear-displacement diagram of steel plate shear walls with pre compression from adjacent frame columns," *The Structural Design of Tall and Special Buildings*, p. e1585, 2019.

[17] Y. Lv, Z. X. Li, and G. X. Lu, "Shear capacity prediction of steel plate shear walls with pre-compression from columns," *The Structural Design of Tall and Special Buildings*, vol. 26, no. 12, p. e1375, 2017.

[18] Y. Lv, D. Wu, Y. H. Zhu et al., "Stress state of steel plate shear walls under compression- shear combination load," *The Structural Design of Tall and Special Buildings*, vol. 27, no. 6, p. e1450, 2018.